Vision Control System for Automated Microassembly

Shashank Tripathi†
Robotics Institute,
Carnegie Mellon University,
Pittsburg, United States of America
shashank.tripathi123@gmail.com

Devesh Ramcharan Jain†
Department of Electronics Engineering,
BITS, Pilani, India
deveshjain94@gmail.com

Himanshu Dutt Sharma
Micro and Nano Assembly and Characterisation Lab,
CEERI, Pilani, India
hdsharma@gmail.com

***Abstract*—In this paper, authors present the development of a completely automated system to perform 3D micromanipulation and microassembly tasks. The microassembly workstation consists of a 3 degree-of-freedom (DOF) MM3A® micromanipulator arm attached to a microgripper, two 2 DOF PI® linear micromotion stages, one optical microscope coupled with a CCD image sensor, and two CMOS cameras for coarse vision. The whole control strategy is subdivided into various vision based routines: manipulator detection and coarse alignment, autofocus and fine alignment of microgripper, target object detection, and performing the required assembly tasks. A section comparing various objective functions useful in the autofocussing regime is included. The control system is built entirely in the image frame, eliminating the need for system calibration, hence improving speed of operation. A micromanipulation experiment performing pickand-place of a micromesh is illustrated. This demonstrates a three-fold reduction in setup and run time for fundamental micromanipulation tasks, as compared to manual operation. Accuracy, repeatability and reliability of the programmed system is analyzed.**

***Keywords*—Micromanipulation, Microassembly, Automation, 3D, Visual Servoing**

I. INTRODUCTION

Serial microassembly [1] largely involves manual operation with high-precision pick-and-place robots [2]. Biological micromanipulations, specifically invitro-fertilization and cell characterization, are still performed by a human operator [3]. Manual operation introduces a degree of risk determined by the operator's abilities such as sense, intelligence, reaction time, fatigue and other physical limitations. This results in increased setup and operation time, with high risk of damage due to human error. A genuine closed loop system is thus essential. In this work, the authors present a closed loop system that can perform microassembly operations. The algorithm iteratively performs two major steps: 1. Bringing the micromanipulator arm in focus and 2. Perfoming the microassembly task.

Several feedback approaches have been proposed in the past for automated microassembly. These can be divided into two major classes: vision-based and vision-force based feedback. Ren et al have proposed a vision based system to automatically insert a micropart into a chip slot [2]. Giouroudi et al [4] have worked towards vison-based automation but have achieved tracking of the end-effector by mounting an LED marker. An external mount can potentially alter micro-movements and negatively affect precision.

† Both authors contributed equally to the manuscript

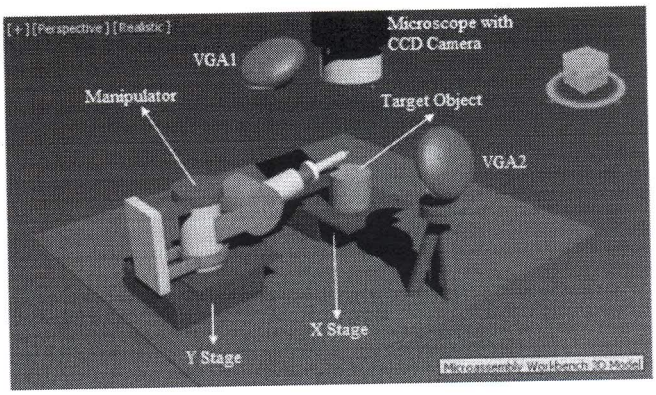

Fig. 1. MM3A® Microassembly Workbench

Other approaches proposed by Kim et al [5], Dionnet et al [6], Bilen et al [3] employ both vision and force feedback. However, to the best of our knowledge, no previous research aims for a reduction in setup and run time for automated micromanipulation.

The paper incrementally developes a fully automated closed-loop micromanipulator control system without any external hardware modifications/mounts. The only necessary human intervention is in defining the system scope in the form of target object to be picked and the destination point where the picked object is to be placed. Section-II briefly outlines the microassembly workcell components and setup. Section-III presents the mathematical model for forward and inverse kinematics of the MM3A® manipulator. Section-IV describes the algorithm flow. Section-V further develops the control strategy by illustrating a micromanipulation experiment. Section-VI shows the experimental results and SectionVII is the conclusion.

II. ELEMENTS OF A MICROASSEMBLY WORKCELL

The microassembly workstation (Fig. 1) was designed for manipulation in 3D space and to perform assembly tasks. The workstation uses a Kliendiek Nanotechnik MM3A micromanipulator, with a microgripper end-effector that has a holding force of up to 1N. The manipulator is a 3 DoF system working in polar coordinates, with two different speed configurations: 10mm/s (Speed A) and 2mm/s (Speed B) and angular resolutions of less than 10^{-7} rad (5nm, 3.5nm and 0.5nm). The manipulator is mounted on a separate 2DoF x-y M-663 Compact Linear Position Stage with 0.6μm resolution,

max speed of 250mm/s and travel range of 18mm ('Y stage' in Fig. 1). A 1 mm diameter micro mesh was placed on another 2DoF x-y stage for experiment and validation ('X stage' in Fig. 1). Cartesian (x, y and z) and spherical coordinate notations (θ, φ and d) used in the paper are defined in Fig 2(a).

The setup was placed under a light microscope with Nikon CF Plan EPI 20x/0.35 objective lens, and was viewed through a CCD camera providing a resolution of 1024x1280 pixels. This microscope is used to obtain a fine, magnified, 2D view of the setup due to its small depth of field property. Two CMOS cameras, each providing a resolution of 640x480 pixels were added to provide a coarse top and side view of the workspace. The control software provides real-time directions to the manipulator and to the position stages. The two CMOS cameras are used for coarse alignment of the manipulator whereas the CCD camera optical system is used for fine alignment and for performing the manipulation tasks.

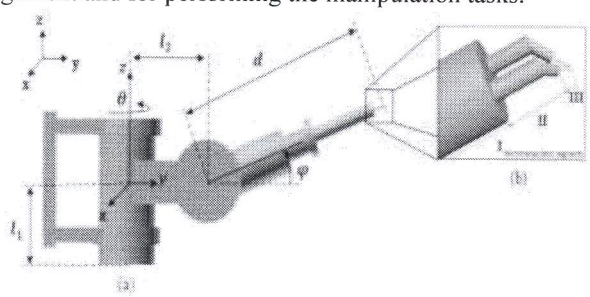

Fig. 2. (a) MM3A® Link - Joint Model, (b) Different Microgripper Segments

III. MATHEMATICAL MODELING OF MICROMANIPULATOR AND MICROMANIPULATOR WORKSPACE

The MM3A® nanomanipulator has three degrees of freedom, and has been represented as a link-joint model in Fig. 2. Using Denavit-Hartenberg convention and taking actual physical dimensions into consideration, the coordinate transformation matrices for the successive links can be written as below:

$$T_{01} = \begin{vmatrix} cos\theta & 0 & sin\theta & l_2 cos\theta \\ sin\theta & 0 & -cos\theta & l_2 sin\theta \\ 0 & 1 & 0 & l_1 \\ 0 & 0 & 0 & 1 \end{vmatrix}$$

$$T_{12} = \begin{vmatrix} cos\phi & 0 & sin\phi & 0 \\ sin\phi & 0 & -cos\phi & 0 \\ 0 & 1 & 0 & 0 \\ 0 & 0 & 0 & 1 \end{vmatrix}$$

$$T_{23} = \begin{vmatrix} 1 & 0 & 0 & 0 \\ 0 & 1 & 0 & 0 \\ 0 & 0 & 1 & d \\ 0 & 0 & 0 & 1 \end{vmatrix}$$

The composite homogeneous transformation matrix is given by,

$$T = T_{01} T_{12} T_{23}$$

$$= \begin{vmatrix} cos\theta cos\phi & sin\theta & cos\theta sin\phi & dcos\theta sin\phi + l_2 cos\theta \\ sin\theta cos\phi & -cos\theta & sin\theta sin\phi & dsin\theta sin\phi + l_2 sin\theta \\ sin\phi & 0 & -cos\phi & -dcos\phi + l_1 \\ 0 & 0 & 0 & 1 \end{vmatrix}$$

Using the forward kinematic relations' first derivative approach, manipulator tip's linear speed relation has been determined. The tip position and speed can be written as,

$$\begin{aligned} X &= 57.1 cos\theta + dcos\theta sin\varphi \\ Y &= 57.1 sin\theta + dsin\theta sin\varphi \\ Z &= 25.4 - dsin\varphi \end{aligned}$$

$$\begin{bmatrix} \dot{X} \\ \dot{Y} \\ \dot{Z} \end{bmatrix} = \begin{bmatrix} -dsin\theta sin\phi - 57.1 sin\theta & dcos\theta cos\phi & cos\theta sin\phi \\ dcos\theta sin\phi - 57.1 cos\theta & dsin\theta cos\phi & sin\theta sin\phi \\ 0 & -dcos\phi & -sin\phi \end{bmatrix} \begin{bmatrix} X \\ Y \\ Z \end{bmatrix}$$

Using the Inverse kinematic relationship the joint variables can be determined as,

$$\theta = atan2(Y, X)$$

$$\phi = atan2((\sqrt{X^2 + Y^2} - 57.1)(25.4 - Z))$$

$$d = (25.4 - Z)/cos\phi$$

IV. MICROASSEMBLY WORKCELL AUTOMATION: SOFTWARE COMPONENTS AND ALGORITHMS

The overall algorithm can be sub-divided into two broad sections: 1) Focusing the end-effector tip 2) Performing microassembly operations

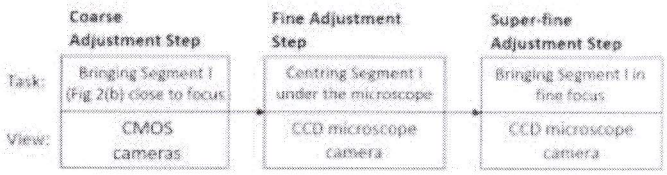

Fig. 3. Algorithm architecture and information flow

A. Focussing the end-effector tip

Bringing the end-effector tip in focus is usually the most time consuming step in automation of microassembly tasks. With a gripping area of 5 to 10 μm^2, the microgripper tip is too fine to be spotted in a direct search approach. The proposed algorithm goes through a series of iterative steps. First, Segment I in Fig 2(b) is brought close to focus in the 'coarse' alignment step. This segment is then centered under the microscope's field-of-view (FOV) in the 'fine' alignment step. The 'super fine' alignment step brings Segment I in fine focus. This segment is then tracked down to Segment II (Fig 2(b)) and Segment III (Fig 2(b)) , while maintaining constant focus.

different stages with the accompanying binary images indicating the number of high intensity pixels.

3) Super-fine adjustment step: An image in focus is characterised by sharp boundaries, distinct internal textures, color gradients and clear edges. The image with the best combination of these features is said to be in 'best' focus amongst other 'near' focus images.

Various focus measure algorithms have been developed in past years. Said Pertuz et al [7] have summarised various focus measure algorithms in their work. These can be Gradient-Based (GRA), Laplacian-Based (LAP), WaveletBased (WAV), Statistics-Based (STA), Tenegrad (TEN) and DCT-Based (DCT). The focus measure (FM) values for a set of 21 images(Table 1) were calculated for all these functions. These images were taken sequentially as the manipulator arm moved across the focal plane from top to bottom (Fig 7). The FM values were plotted against the image number to obtain a focus curve. A desirable focus measure curve should observe a sharp peak at the best focus in addition to being computationally inexpensive. The best three curves, based on the presence of a sharp peak at focus, unique local maximum, and least calculation time have been picked and laid out for analysis (Table 1 and Fig 8). The FM using Tenegrad Variance clearly had an upper hand in accurately pointing out the best focus image in the least amount of time. Eqn 1 gives the expression for calculating the Tenegrad Variance. This outputs a nxm matrix with the sum of pixel values of the sobel filtered image(nxm) along the X and Y directions. The variance of this matrix is used as a single value indicator of focus measure.

$$F_{nxm} = S_x(x,y,z)^2 + S_y(x,y,z)^2 \qquad (1)$$

where,

$$S_x(z) = I_{nxm}(z) * \begin{bmatrix} 1 & 2 & 1 \\ 0 & 0 & 0 \\ -1 & -2 & -1 \end{bmatrix},$$

$$S_y(z) = I_{nxm}(z) * \begin{bmatrix} -1 & 0 & 1 \\ -2 & 0 & 2 \\ -1 & 0 & 1 \end{bmatrix}$$

The manipulator thus moves in the φ direction calculating the Tenegrad Variance values at each step until it reaches the maximum. Once Segment I in the manipulator arm is brought under focus, the algorithm tracks the arm until it reaches the tip (Segment III).

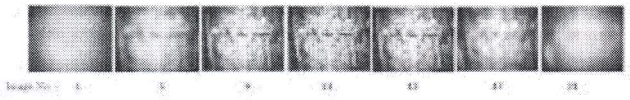

Fig. 7. Image sequence for obtaining focus measures

V. EXPERIMENTS WITH MICROMESH

A. Target Object Coordinates and Orientation

Microassembly task such as pick and place of micro mesh were performed in order to demonstrate the utility of the proposed algorithm. The mesh is characterized by intersecting lines. Applying sobel edge detection gives the coordinates and

TABLE I. FOCUS MEASURE TABLE

Image Number	TEN FM	WAV FM	GRA FM
1	8000	0.3359	26.4553
5	4000	0.3029	26.451
9	21648000	0.7149	26.7688
11 (Best focus)	77697000	1.0848	26.9905
13	8022000	0.4824	26.7232
17	107000	0.2874	26.3934
21	6000	0.2356	26.6581
Time Taken (sec)	0.132	0.121	0.304

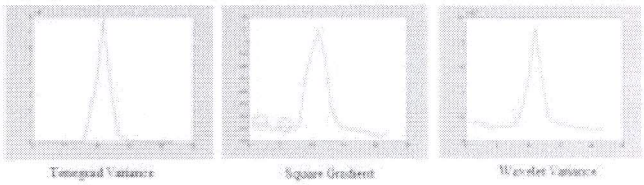

Fig. 8. Plots of various focus measure functions. TEN FM is the winfigner due to sharp peak at best focus and a single maximum. Other FM functions either have multiple local maxima or are more time-consuming

orientation of these intersecting lines. Any such line, parallel to the microgripper tip, can be used for picking the object. For better control, when prompted, the user is allowed to select a region of choice on the image, best suited for pick up (yellow rectangle in Fig. 10(a)). The selected region is processed and a point is marked for approach by the gripper to pick the micromesh (yellow cross in Fig. 10 (b)). In successive steps, the gripper central point (Green Cross in Fig. 10(c)), obtained in Section IV, is matched with this point for pick up (Fig. 10(c) and (d)).

B. Collision Avoidance

In usual collision avoidance strategies, a rectangular region about twice larger than the obstacle is assumed around the obstacle. The manipulator is then allowed to move as long as it stays outside this region [3]. On the contrary, in the proposed collision avoidance scheme, the manipulator is first brought under focus and then moved out of microscope's FOV using PI®stage (Y stage in Fig 1), to allow placement of the target object under the microscope FOV using another PI®stage (X stage in Fig 1). The micromanipulator is then moved back to the original location to perform microassembly operation but has a vertical clearance of about 1mm above the micromesh. Once the tip point and the pick up coordinates in x-y plane on the mesh are perfectly matched, the gripper tip is slowly brought down in focus. As soon as the gripper touches the micromesh, the actuators close the gripper arm, picking the micromesh. Successive pick and place experiments are even quicker because the end-effector tip is already in focus

VI. RESULTS AND DISCUSSION

A. Experimental Testing of Automation Program

Program segments for automatic joint motions, reaching the desired orientation, end-effector centering, autofocusing, tip

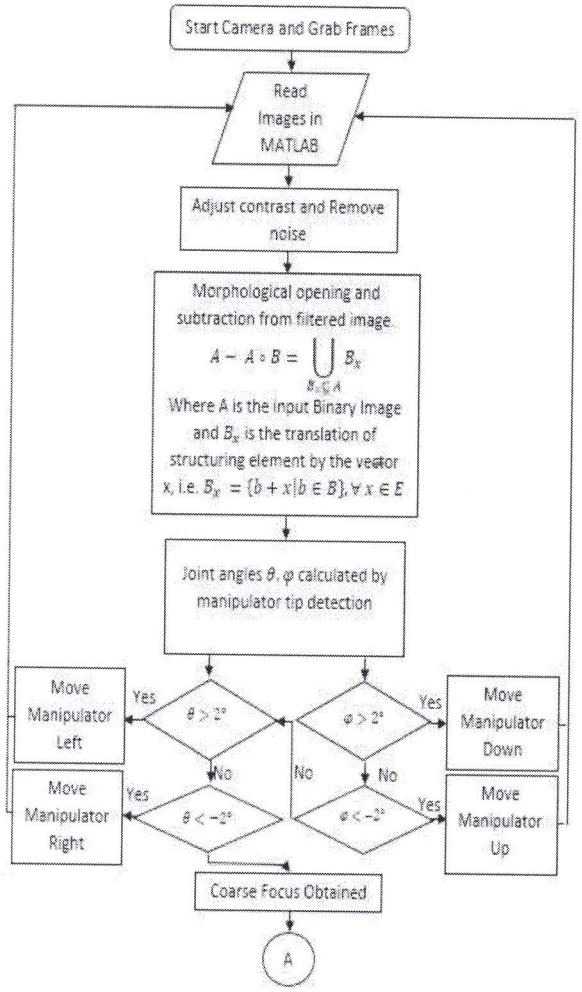

Fig. 4. Coarse Focus Flowchart

The following sections describe the coarse, fine and superfine alignment steps and Fig. 3 illustrates the algorithm architecture and information flow between components.

1) Coarse adjustment step: Raw RGB images are obtained as inputs from the top camera (Fig 5(a)). After contrast enhancement, morphological opening of the image is performed (Fig 5(b), which is subtracted from the original image to highlight the foreground subject's (i.e. the manipulator's) features (Fig 5(c)). Edges are identified using a generalised Hough transform, and the top most point in the edge is labeled as the tip. The line passing through the center of the manipulator body and the center of the microscope's light spot is denoted as 0°(Fig 5(d)). Once the reference and the manipulator arm tip is defined, the joint angle in the x-y plane (θ in Fig 5(d)) can be obtained. The same process is repeated for images obtained from the side camera and the joint angles are obtained in the y-z plane (φ).

As described in the flowchart(Fig 4), in coarse adjustment, an offset of 2° is provided on both sides of the destination point. Therefore, for achieving control of the endeffector's measured position in world spherical polar coordinates $[\theta_m^{(w)}, \phi_m^{(w)}]^T$, the desired coordinates $[\theta_d^{(w)}, \phi_d^{(w)}]^T$ (where $\theta_d^{(w)} = 0° \pm 2°$ *and* $\phi_d^{(w)} = 0° \pm 2°$) are matched with

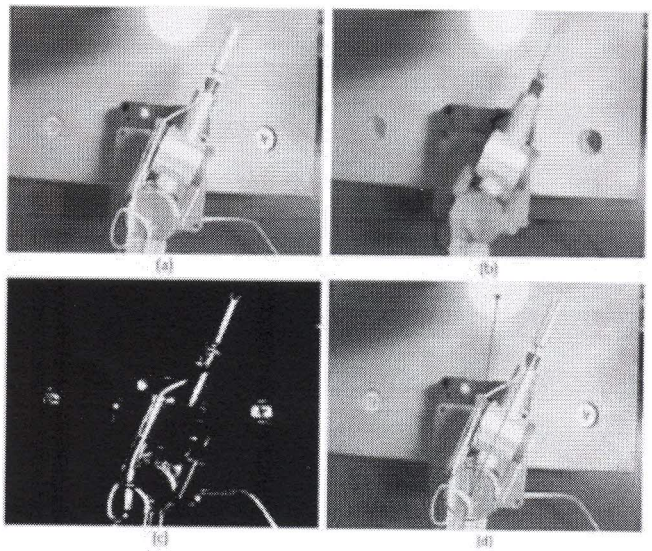

Fig. 5. (a) Raw RGB Image, (b) Morphologically Opened)Image, (c Manipulator Segmented, (d) Manipulator Tip marked (green dot) with respect to reference point (blue dot)

$[\theta_m^{(w)}, \varphi_m^{(w)}]^T$ utilizing coarse manipulator movement (Speed A). In this way, the manipulator joints are given inputs depending on the manipulator arm's current position coordinates in both horizontal and vertical directions to move it into the critical region of $\pm 2°$. The algorithm then shifts from coarse to fine motion (Speed B) as soon as the manipulator arm enters this middle band $-2° < \theta_m^{(w)} < 2°, -2° < \varphi_m^{(w)} < 2°$.

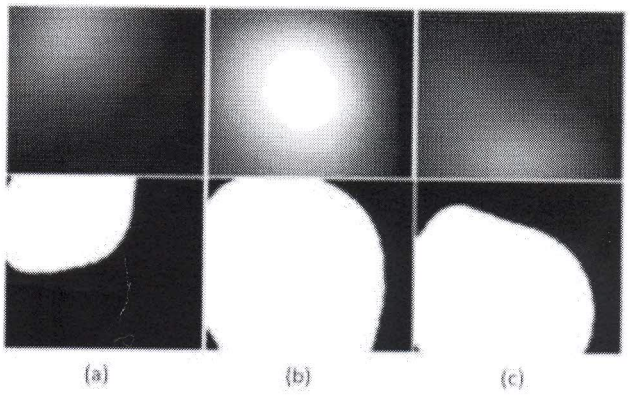

Fig. 6. Raw and processed images at different stages of the 'fine' adjustment step. (b) has the largest proportion of high intensity pixels implying that the manipulator is centered in microscope's FOV

2) Fine adjustment step: In this section, the vision system switches to the microscope's CCD camera along with a decrease in manipulator speed. The manipulator arm is said to be centered in the microscope's FOV when there is a region of high specular reflection of the microscope light from the manipulator arm surface. This position is characterized by the number of high intensity pixel values. The total number of high intensity pixels are maximized over various frames as the manipulator arm continues to move towards 0°. The position with maximum brightness is thus found. Fig. 6 illustrates the

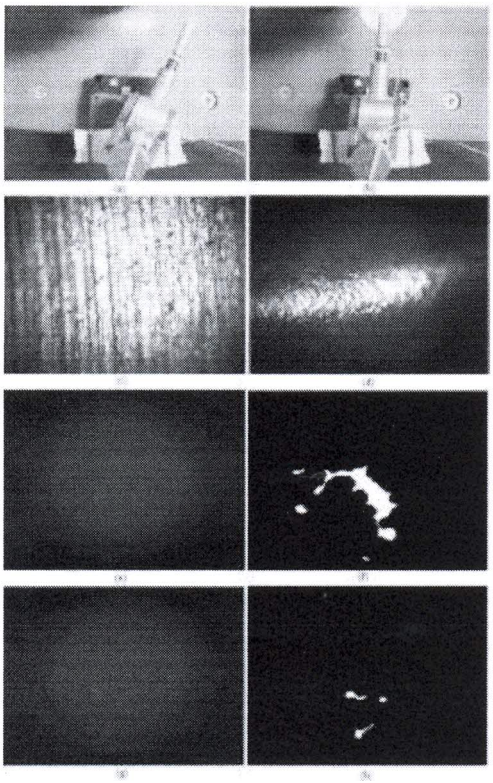

Fig. 9. (a) Initial position, (b) Centered manipulator after 'coarse' and 'fine' adjustment step, (c) Segment I under focus, (d) Segment II under focus, (e) Tracking Segment III (f) Binary segmentation of Segment III, (g) Tip in focus,
(h) Binary segmentation of manipulator tip

focusing, pick and place tasks were performed successfully. Fig. 9 and 10 display images acquired by the camera during the test run. Fig. 9 shows the 'autofocus' algorithm at work, starting with a random, user-defined initial position shown in Fig. 9(a). Fig. 9(b) shows the centered Segment I after the 'fine' alignment step. Fig 9(c) and (d) show focused Segment I and Segment II respectively, as they were tracked. Fig. 9(e), (f) show the RGB image of Segment III and its corresponding binary segmentation whereas Fig. 9(g), (h) show the manipulator tip. Fig. 10 shows the pick-n-place operation. The user selection of the required pick-up area is shown as a yellow box in Fig. 10(a). The exact pick-up coordinates, within the area defined by the user, have been marked (yellow cross in Fig. 10(b)). Fig. 10(c) and (d) show the pick-up point on the mesh (yellow cross) and the current position of the microgripper tip (green cross) which are aligned together within an acceptably precise range of error (5μm in both x and y directions) (see Fig. 10(d)). A faint silhouette of the microgripper can be seen in Fig. 10(e) above the desired mesh pick-point. As the mesh is picked up by the microgripper (Fig. 10(f)), it moves above the focal plane of the microscope, hence becoming de-focused, as can be seen in Fig. 10(g) after successful pickup. The side view, Fig. 10(h), clearly shows the micromesh in picked-up position. Next, the placing operation is initiated by bringing the destination place point on the PI® Stage under focus (Fig. 10(i)). The picked-up mesh is further raised up for added safety and is brought back over the place-point (Fig. 10(j)). The mesh is released over the requied destination point by opening the microgripper end-effector hair. The mesh comes back under focus indicting a successful place operation (Fig. 10(k)).

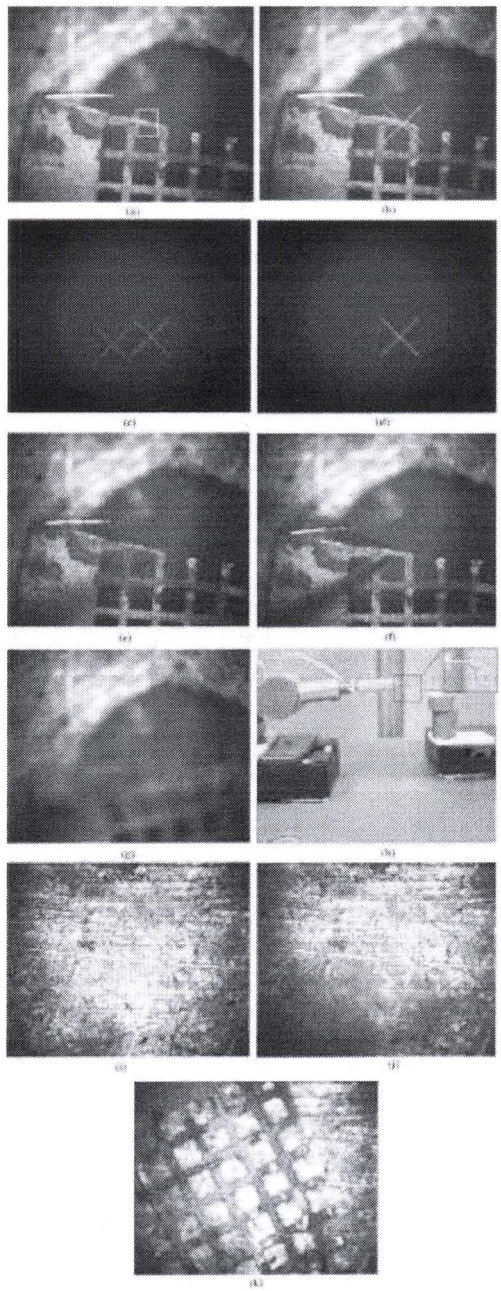

Fig. 10. (a) User selecting the pick region on the micromesh, (b) Yellow cross indicating the pick-up point, (c) Aligning the microgripper to match with the pick point, (d) Alignment achieved, (e) Faint silhouette of gripper visible over the micromesh, (f) Microgripper gripping the micromesh, (g) Micromesh picked up, (h) Side View of the manipulator holding the micromesh, (i) Drop Position, (j) Faint silhouette of mesh above the drop location, (k) Mesh Dropped

B. Program Performance Analysis

The program performance analysis measures the timing and accuracy of the program. Effects of environment changes and other contingency variables have also been discussed.

TABLE II. TIME TAKEN FOR INDIVIDUAL TASKS

Task	Time taken (sec)	Cumulative (sec)
Initialisation	66	66
Coarse	14	80
Fine	8	88
Superfine	32	120
Tracking end-effector	258	378
Pick and Place	353	741

1) Timing Analysis: The mean cycle-time for centering and auto focusing the manipulator tip by a human operator is approximately 30 minutes. An overall time of 40 to 60 minutes is required to complete the entire pick-n-place operation, provided the person has good concentration and skills to avoid damage to the system. The proposed algorithm based routine performs the same job much faster: 6 minutes 18 seconds are taken for auto-focusing whereas 12 minutes 21 seconds are taken for overall completion of the task. Table II delineates the time taken (in seconds) for completing different tasks in the automated micromanipulation regime.

2) Accuracy: The pick-up and the tip point coordinates were matched within a precision of 5μm and below depending upon the microscope magnification factor. A high-precision optical micrometer was used to measure this metric. For successive pick-and-place of multiple objects, there is no need to rerun the autofocus regime since the manipulator tip is already in focus. This further reduces the run time for successive experiments. However, after continuous repetitions, for upto 5 successive cycles, the 'superfine' step is rerun to counter the effects of joint backlash errors. The nano-motors inside the manipulator joints also have the possibility of 'stepmissing' which affects the iterative process.

3) Environment controls: The program is repeatable as long as the the experiment is performed in controlled environmental conditions. The repeatability is enhanced in clean room conditions, incorporating better and more accurate peizomotors with a reduced possibility of joint back-lash and stepmissing in the manipulator robot. Performance was tested by varying brightness levels between 1500 to 5000 lumens, in steps of 500. The pick and place experiment was thus found to be robust to changes in lighting conditions. Experiments were also conducted with different initial orientations for the manipulator and the program was observed to be stable to intensity changes caused due to light reflections.

VII. CONCLUSION

The development presented in the paper provides a holistic approach to successfully automate a flexible, programmable, articulated robotic arm for complex operations in micro assembly of systems and components. A new iterative search and track algorithm is proposed to keep the manipulator endeffector in focus. Although the algorithm has been developed for MM3A micromanipulator, it can be similarly extended to any 3-6 DoF micromanipulator. The autofocusing algorithm proposed in this paper aims to reduce the time taken in automatic micromanipulation experiments. Although several automation schemes have been presented [2] [3], none aim at improving the timing efficiency of the developed system. Our approach introduces a three-fold reduction in setup and run time as has been demonstrated in the paper.

ACKNOWLEDGMENT

The authors would like to thank CSIR for funding this project ESC112. We would also like to extend our deep sense of gratitude to Mr Sunny, Project Staff and Mr Talebar Singh, Technical Staff and group leader Dr. Bhanu Prasad for their valuable suggestions and support.

REFERENCES

[1] K. F. Bohringer, R. S. Fearing, and K. Y. Goldberg, "Microassembly," Handbook of Industrial Robotics, Second Edition, pp. 1045–1066, 2007.

[2] L. Ren, L. Wang, J. K. Mills, and D. Sun, "3-d automatic microassembly by vision-based control," in 2007 IEEE/RSJ International Conference on Intelligent Robots and Systems. IEEE, 2007, pp. 297–302.

[3] H. Bilen and M. Unel, "Micromanipulation using a microassembly workstation with vision and force sensing," in International Conference on Intelligent Computing. Springer, 2008, pp. 1164–1172.

[4] I. Giouroudi, "Design of a microgripping system with visual and force feedback for mems applications," in MEMS Sensors and Actuators, 2006. The Institution of Engineering and Technology Seminar on. IET, 2006, pp. 243–250.

[5] B. Kim, H. Kang, D.-H. Kim, G. T. Park, and J.-O. Park, "Flexible microassembly system based on hybrid manipulation scheme," in Intelligent Robots and Systems, 2003.(IROS 2003). Proceedings. 2003 IEEE/RSJ International Conference on, vol. 2. IEEE, 2003, pp. 2061–2066.

[6] F. Dionnet, D. S. Haliyo, and S. Regnier, "Autonomous micromanipulation using a new strategy of accurate release by rolling," in Robotics and Automation, 2004. Proceedings. ICRA'04. 2004 IEEE International Conference on, vol. 5. IEEE, 2004, pp. 5019–5024.

[7] S. Pertuz, D. Puig, and M. A. Garcia, "Analysis of focus measure operators for shape-from-focus," Pattern Recognition, vol. 46, no. 5, pp. 1415–1432, 2013.